

Three-dimensional topological crystalline insulator without spin-orbit coupling in nonsymmorphic photonic metacrystal

Zhide Yu(余智德) and Lingbo Xia(夏凌波)

Citation: Chin. Phys. B, 2024, 33 (**10**): 104209. DOI: 10.1088/1674-1056/ad6a3e
Journal homepage: http://cpb.iphy.ac.cn; http://iopscience.iop.org/cpb

What follows is a list of articles you may be interested in

Interface state-based bound states in continuum and below-continuum-resonance modes with high-*Q* factors in the rotational periodic system

Jialing Yang(杨嘉玲), Aoqian Shi(史奥芊), Yuchen Peng(彭宇宸), Peng Peng(彭鹏), and Jianjun Liu(刘建军)
Chin. Phys. B, 2024, 33 (**8**): 084206. DOI: 10.1088/1674-1056/ad4630

Topological edge and corner states of valley photonic crystals with zipper-like boundary conditions

Yun-Feng Shen(沈云峰), Xiao-Fang Xu(许孝芳), Ming Sun(孙铭), Wen-Ji Zhou(周文佶), and Ya-Jing Chang(常雅箐)
Chin. Phys. B, 2024, 33 (**4**): 044203. DOI: 10.1088/1674-1056/ad1e6a

High-efficiency ultra-fast all-optical photonic crystal diode based on the lateral-coupled nonlinear elliptical defect

Daxing Li(李大星), Kaizhu Liu(刘凯柱), Chunlong Yu(余春龙), Kuo Zhang(张括),Yueqin Liu(刘跃钦), and Shuai Feng(冯帅)
Chin. Phys. B, 2024, 33 (**3**): 034215. DOI: 10.1088/1674-1056/ad0117

Simultaneous guidance of electromagnetic and elastic waves via glide symmetry phoxonic crystal waveguides

Lin-Lin Lei(雷林霖), Ling-Juan He(何灵娟), Qing-Hua Liao(廖清华), Wen-Xing Liu(刘文兴), and Tian-Bao Yu(于天宝)
Chin. Phys. B, 2024, 33 (**3**): 034202. DOI: 10.1088/1674-1056/ad0ec7

High-performance chiral all-optical OR logic gate based on topological edge states of valley photonic crystal

Xiaorong Wang(王晓蓉), Hongming Fei(费宏明), Han Lin(林瀚), Min Wu(武敏), Lijuan Kang(康丽娟), Mingda Zhang(张明达), Xin Liu(刘欣), Yibiao Yang(杨毅彪), and Liantuan Xiao(肖连团)
Chin. Phys. B, 2023, 32 (**7**): 074205. DOI: 10.1088/1674-1056/accb41

Three-dimensional topological crystalline insulator without spin–orbit coupling in nonsymmorphic photonic metacrystal

Zhide Yu(余智德) and Lingbo Xia(夏凌波)†

School of Physics and Electronics, Hunan University, Changsha 410082, *China*

(Received 10 July 2024; revised manuscript received 28 July 2024; accepted manuscript online 2 August 2024)

By including certain point group symmetry in the classification of band topology, Fu proposed a class of three-dimensional topological crystalline insulators (TCIs) without spin–orbit coupling in 2011. In Fu's model, surface states (if present) doubly degenerate at $\bar{\Gamma}$ and $\bar{M}$ when time-reversal and C_4 symmetries are preserved. The analogs of Fu's model with surface states quadratically degenerate at $\bar{M}$ are widely studied, while surface states with quadratic degeneracy at $\bar{\Gamma}$ are rarely reported. In this study, we propose a three-dimensional TCI without spin–orbit coupling in a judiciously designed nonsymmorphic photonic metacrystal. The surface states of photonic TCIs exhibit quadratic band degeneracy in the (001) surface Brillouin zone (BZ) center ($\bar{\Gamma}$ point). The gapless surface states and their quadratic dispersion are protected by C_4 and time-reversal symmetries, which correspond to the nontrivial band topology characterized by Z_2 topological invariant. Moreover, the surface states along lines from $\bar{\Gamma}$ to the (001) surface BZ boundary exhibit zigzag feature, which is interpreted from symmetry perspective by building composite operators constructed by the product of glide symmetries with time-reversal symmetry. The metacrystal array surrounded with air possesses high order hinge states with electric fields highly localized at the hinge that may apply to optical sensors. The gapless surface states and hinge states reside in a clean frequency bandgap. The topological surface states emerge at the boundary of the metacrystal and perfect electric conductor (PEC), which provide a pathway for topologically manipulating light propagation in photonic devices.

Keywords: topological crystalline insulator, nonsymmorphic photonic metacrystal

PACS: 42.70.Qs, 78.67.Pt, 73.43.Nq **DOI:** 10.1088/1674-1056/ad6a3e

1. Introduction

Photonic crystals were proposed in the 1980s, which are constructed by embedding periodical structural defects into a material.[1–3] With a carefully designed structure unit, photonic crystals will show bandgaps in the frequency spectrum. Surface states in the frequency bandgaps appearing at the interface between photonic crystals and material are localized electromagnetic modes.[4] In contrast to the bulk states with electromagnetic fields distributed throughout the material, the surface states are usually confined to a thin layer near the interface. Its highly confined electromagnetic field distribution gives rise to unique properties distinct from bulk states, such as higher sensitivity to the changes in the environment at the interface. The manipulation of light propagation and emission properties is widely studied by embedding structure defects into the bulk of photonic crystals.[5–7] Nevertheless, controlling surface states as a way of manipulating the propagation of light is rarely explored.[8,9]

The interest in surface states has attracted rapid attention since the discovery of topological insulators in condensed matter systems.[10,11] In recent decades, with the extension of topological physics to photonic systems, various photonic analogs of topological insulators have been discovered.[12–17] The topological insulators are insulating in the bulk and supporting unidirectional transported surface states at the boundary. Their nontrivial topological properties are induced by band inversion under strong spin–orbit coupling with preserving of time-reversal symmetry, which leads to spin-polarized gapless Dirac surface states.[10,18] However, the intrinsic lack of electron spin in photonic system forced to construction of photonic pseudospins to mimic the behaviours of electron spin.[15] Such photonic pseudospin usually requires extra symmetries, such as the electromagnetic duality of the structure unit, which leads to topological surface states only emerging at the internal boundary between two identical photonic topological insulators with opposite settings.[14,19–21]

Meanwhile, a class of three-dimensional (3D) TCIs was proposed by Fu in 2011, in which the nontrivial band topology is protected by C_4 and time-reversal symmetry.[22] Especially, the spin–orbit coupling is not a necessity for TCIs, which is right suited in photonic systems. Compared with the topological surface states of topological insulators exhibiting Dirac degeneracy, the topological surface states (if present) of TCIs exhibit a quadratic degeneracy at $\bar{\Gamma}$ and $\bar{M}$ point. The Fu's model with quadratic degeneracy of topological surface states at $\bar{M}$ point is widely studied,[23–28] nevertheless, the realization of TCIs with topological surface states quadratically degenerated at $\bar{\Gamma}$ point in nonsymmorphic photonic metacrystal is still unexploited. Here, we propose a realistic nonsymmorphic photonic metacrystal for the realization of 3D TCIs. The gapless topological surface states exhibit quadratic band crossing protected by C_4 and time-reversal symmetry at $\bar{\Gamma}$ point.

†Corresponding author. E-mail: lingboxia@hnu.edu.cn

© 2024 Chinese Physical Society and IOP Publishing Ltd

The nontrivial band topology of the photonic TCI is revealed by the Zak phase along bent loops connecting two C_4-invariant points. Meanwhile, zigzag feature of gapless surface states appears along lines from $\bar{\Gamma}$ to the surface BZ boundary is due to the composite operators,[29–31] which is constructed by production between glide symmetries and time-reversal symmetry and ensure doubly degenerated states in the (001) surface BZ boundary. Different from previous photonic topological insulator with surface states existing at the internal boundary between two identical photonic topological insulators with opposite settings, the topological surface states appear at the boundary of the metacrystal and PEC, which provide a pathway for topologically manipulating light propagation at the surface of photonic TCIs. Moreover, the high order hinge states exhibit continues dispersions residing in the bandgap are explored, where the electric fields highly confined at the hinge may apply to optical sensors.

2. Model and method

The unit cell of the metacrystal is constructed by two identical metallic splitting resonant rings embedded into a host material with a dielectric constant of 2.2, as shown in Fig. 1(a). The periods of the metacrystal are $p_x = p_y = 4$ mm, $p_z = 4.5$ mm, and geometrical parameters of the metallic splitting resonant rings are given as $H = 3.75$ mm, $W = 0.2$ mm, $L = 1.5$ mm, $R = 0.3$ mm. The photonic metacrystal corresponds to a simple tetragonal lattice with a nonsymmorphic space group $P4bm$ (No: 100),[32] which includes two glide mirror operations involving half lattice translation, $\tilde{M}_x : (x,y,z) \to (-x,1/2+y,z)$, $\tilde{M}_y : (x,y,z) \to (1/2+x,-y,z)$. The tilde above the mirror operation symbol denotes that it is a nonsymmorphic symmetry operator. The photonic metacrystal possess four-fold rotation symmetry $C_4 : (x,y,z) \to (-y,1/2+x,z)$ with rotation axis $(0,0,z)$, where the half lattice translation along the y direction have no physical meaning since it can be eliminated by choosing another rotation axis $(1/4,-1/4,z)$ (see supplement material for more details). The point group of the metacrystal is C_{4v} (or 4 mm in Hermann–Mauguin notation). The metacrystal can be fabricated by standard printed circuit board (PCB) technique, while the host material is made of F4BM and the thickness of the copper-clad is 0.035 mm. In this paper, the theoretical results are calculated by CST MICROWAVE STUDIO. In the microwave region, the metallic components are considered as PEC. The tetragonal BZ is boxed by gray lines and the surface BZ in the (001) and (100) planes are colored by dark and light gray, respectively, where the related high symmetric points are indicated nearby, as shown in Fig. 1(b). The bulk band spectrum along high symmetry lines is presented in Fig. 1(c), which shows a clean frequency bandgap from 10.1 GHz to 10.9 GHz offering an ideal platform for the studying of surface states.

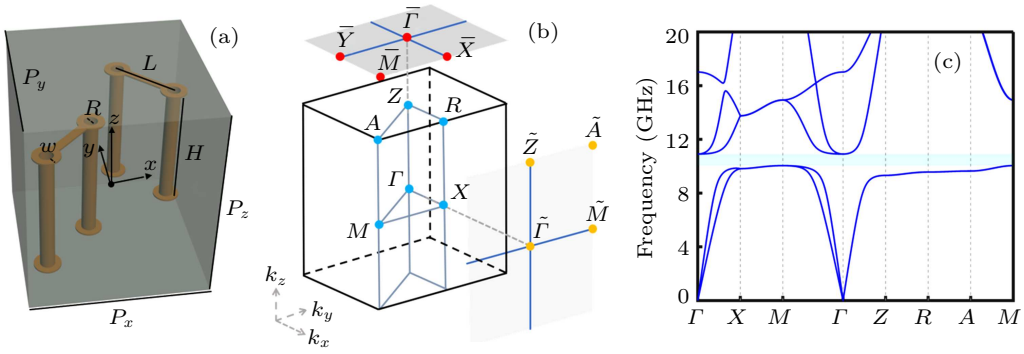


Fig. 1. (a) Unit cell of the photonic metacrystal. The periods of the metacrystal are $p_x = p_y = 4$ mm and $p_z = 4.5$ mm, respectively. The geometrical parameters of two metallic splitting resonant rings are given as $H = 3.75$ mm, $W = 0.2$ mm, $L = 1.5$ mm, $R = 0.3$ mm, and the thickness of the metallic components is set as 0.035 mm. (b) BZ of the tetragonal photonic metacrystal. The reduced BZ are boxed by gray lines and the (001) and (100) surface BZ are denoted by dark and light gray color. The corresponding high symmetry points are indicated nearby. (c) The bulk band spectrum along high symmetry lines. The bulk states are denoted by blue lines, which show a clean bandgap from 10.1 GHz to 10.9 GHz being marked with cyan color.

3. Results and discussion

3.1. Gapless and quadratically degenerated surface states

Firstly, the topological surface states with gapless features and quadratic degeneracy at $\bar{\Gamma}$ are protected by C_4 and time-reversal symmetries. To describe the surface states in the (001) plane, we construct a supercell consisting of 10 unit cells along the y direction. Periodic boundary conditions are applied to the x and y directions, and the perfect electric conductor boundary condition is applied to two sides of the supercell along the y direction. The band spectrum along the line $(-\bar{X})$–$\bar{\Gamma}$–$\bar{X}$ (the line along k_x axis in the (001) surface BZ) is shown in Fig. 2(a), where the blue lines indicate surface states and black lines represent the projected bulk states. The surface states in the bandgap connect the lower and upper bulk states forming a gapless feature. A quadratic band crossing occurs at $\bar{\Gamma}$ point as highlighted by the red point in Fig. 2(a), which is a hallmark of TCIs. The surface states exhibiting gapless features among bandgap and quadratic band crossing at $\bar{\Gamma}$ point are topologically protected by C_4 and time-reversal symmetries. To unveil the bulk topology, we calculate the Zak phase along noncon-

tractible bent loops at constant k_z plane.[25] The gray region restricted in $\{k_x = k_y \geq 0 \cup k_x = -k_y \geq 0, k_z \in [-\pi/p_z, \pi/p_z]\}$ are horizontally sliced into bent loops connecting two C_4-invariants points with constant k_z, such as loops of M–Γ–M in $k_z = 0$ plane and A–Z–A in $k_z = \pi/p_z$ plane, as shown in the inset of Fig. 2(b), where the C_4-invariant points refer to two momenta points which are invariant under 4-fold rotation in the momentum space, up to a reciprocal lattice vector. The Zak phases of the 1st and 2nd bulk bands below the bandgap along bent loops are calculated by utilizing the Wilson loop method (see supplement material for more details about Zak phase calculations). The Zak phase at a given k_z indicates the geometric phase acquired along the bent loops in the constant k_z plane. The spectral flow of Zak phases of the 1st and 2nd bulk bands are plotted against k_z in Fig. 2(b). With preserving of C_4 and time reversal symmetries, the Zak phases of the two bulk states below the bandgap possess opposite signs for all k_z and are quantized to 0 and π (mod 2π) at $k_z = \pi/p_z$ and $k_z = 0$ plane, respectively. Importantly, the Zak phase interpolate across the full ranges $(-\pi, \pi]$ leads to spectral flow when k_z increasing from $-\pi/p_z$ to π/p_z, which is a definite hallmark of the three-dimensional TCIs phase. Those nontrivial Zak phases are characterized by Z_2 topological invariant $\nu_0 = 1$, which coincide with the topological nontrivial surface states featured with gapless and quadratic dispersion[25,28] (see supplement material for more details).

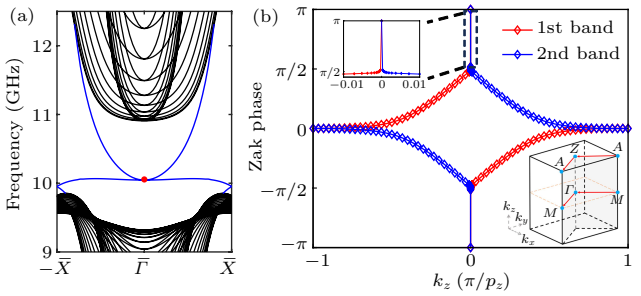


Fig. 2. (a) The band spectrum along line $(-\bar{X})$–$\bar{\Gamma}$–$\bar{X}$ in the (001) surface BZ. The blue and black lines represent the surface states and projected bulk states, respectively. The quadratic degeneracy at $\bar{\Gamma}$ is denoted by red point. (b) The spectral flow of Zak phases of two bulk states below bandgaps. By slicing the gray region horizontally into bent loops connecting two C_4-invariant points as shown in the inset, the Zak phases are calculated along the bent loops in the constant k_z plane for $k_z \in [-\pi/p_z, \pi/p_z]$. Two typical bent loops M–Γ–M and A–Z–A in $k_z = 0$ and $k_z = \pi/p_z$ plane are highlighted by red lines. The Zak phases show dramatical changes in the range $k_z \in [-0.01, 0.01]$ as plotted in the inset.

3.2. Zigzag feature of the surface states

Secondly, the zigzag feature of the surface states in (001) surface BZ is interpreted from a symmetry perspective. Since the supercell belongs to the point group C_{4v}, we only need to examine the degeneracy along a typical high symmetry line $\bar{X}$–$\bar{M}$ to interpret the double degeneracy at (001) surface BZ boundary. We construct composite operators $S_i = \tilde{M}_i \times T$, $(i = x, y)$, which is formed by the production of time-reversal operation (T) and glide refection operation ($\tilde{M}_i$).[31,33,34] Given an arbitrary Bloch state $|\psi\rangle$ of the photonic supercell, the time-reversal symmetry acted on the Bloch state leads to a complex conjugation $T|\psi\rangle = |\psi\rangle^*$. Two successive composite operations S_y acting on the Bloch state $|\psi\rangle$ give rise to a spatial primitive translation,

$$S_y^2 |\psi\rangle = \left(\tilde{M}_y \times T\right)^2 |\psi\rangle = t_{100} |\psi\rangle = e^{ik_x p_x} |\psi\rangle, \quad (1)$$

where t_{100} is primitive translation along the x direction. Given an arbitrary Bloch state $|\psi\rangle$ at $(\pi/p_x, k_y)$ in high symmetry line $\bar{X}$–$\bar{M}$, $S_y|\psi\rangle$ is a new state at $(\pi/p_x, k_y)$. The high symmetry line $\bar{X}$–$\bar{M}$ with $k_x = \pi/p_x$ is invariant under composite operation S_y, which yields,

$$S_y^2 = e^{ik_x p_x}\big|_{k_x = \pi/p_x} = -1. \quad (2)$$

The composite operation S_y is an antiunitary operator along high symmetry line $\bar{X}$–$\bar{M}$, which provides a photonic analog of Kramers theorem for fermions ensuring doubly degenerated surface states along $\bar{X}$–$\bar{M}$. A similar analysis applies to S_x which ensures doubly degenerated surface states along $\bar{Y}$–$\bar{M}$. Therefore, the surface states in (001) surface BZ boundary are all doubly degenerate. The band spectrums along high symmetry lines in the surface BZ are illustrated in Fig. 3(a), where the bulk and surface states are denoted by black and blue lines, respectively. Since the surface states are doubly degenerated at $\bar{\Gamma}$ point and surface BZ boundary, the surface states exhibit gapless and zigzag features along the line from $\bar{\Gamma}$ point to an arbitrary point in the (001) surface BZ boundary, such as the surface states along $\bar{\Gamma}$–$\bar{X}$ and $\bar{\Gamma}$–$\bar{M}$ highlighted by bold blue lines shown in Fig. 3(a).

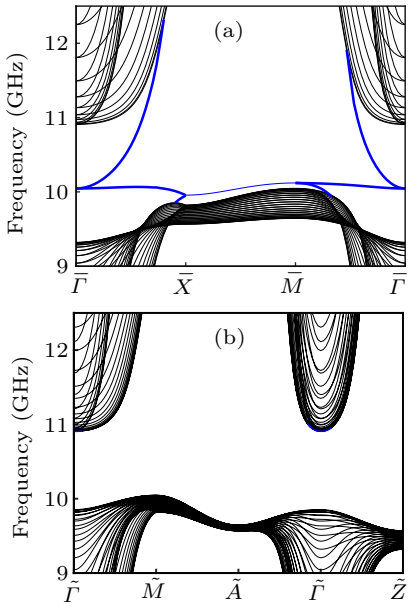


Fig. 3. (a) Band spectrum along high symmetry lines in the (001) surface BZ. The blue and black lines represent the surface states and projected bulk states. The surface states along $\bar{\Gamma}$–$\bar{X}$ and $\bar{M}$–$\bar{\Gamma}$ are highlighted by bold blue lines which exhibit zigzag feature. (b) Band spectrum along high symmetry lines in the (100) surface BZ. The blue and black lines represent the surface states and projected bulk states.

Similarly, to analyze the surface states in the (100) surface BZ, a supercell is constructed by stacking the metacrystal unit with 10 layers along the x direction. Periodic boundary conditions are applied to the y and z directions, and the perfect electric conductor boundary condition is applied to two sides of the supercell along the x direction. In general, the topological surface states of TCIs emerge at high symmetry crystal surface, and the low-symmetry crystal surface does not support robust surface states. The supercell along the x direction has no gapless surface states due to the lack of crystalline symmetry as the band spectrum along high symmetry lines in (100) surface BZ illustrated in Fig. 3(b).

3.3. High order hinge states

Moreover, the high order hinge states are explored by arranging the metacrystal unit into an 8×8 array along the x and y directions and one layer of metacrystal unit in the y direction. Periodic boundary conditions are applied to the y direction, and the metacrystal array is surrounded with air in the x and y directions (open boundary condition in the x and y directions).

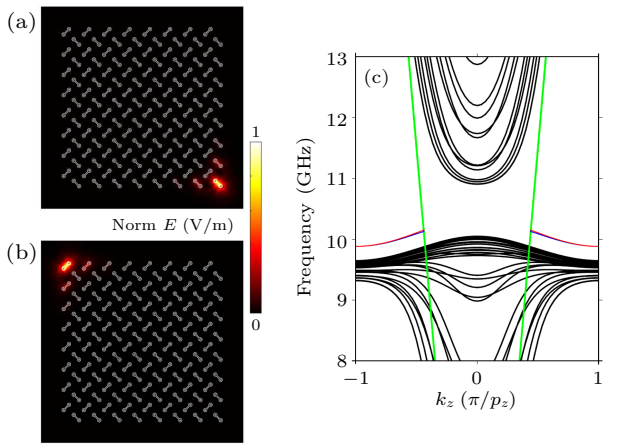


Fig. 4. (a)–(b) The top view of normalized absolute value of electrical field (norm E) distribution of two high order hinge states at $k_z = \pi/p_z$. (c) Band spectrum along the z direction. The black lines represent the projected bulk states. The green lines denote the light cone. The blue and red lines represent two high order hinge states, where the field distributions are shown in panels (a) and (b), respectively. The metacrystal units are arranged into an 8×8 array along the x and y directions, where periodical boundary conditions are applied to the z direction and metacrystal array is surrounded with air in the x and y directions. There are two high order hinge states continuously distributed in the bandgap as k_z various from $-\pi/p_z$ to π/p_z and until connected to the light cone.

The band spectrum as k_z varies from $-\pi/p_z$ to π/p_z are shown in Fig. 4(c), where the black and green lines indicate the projected bulk states and light cone, the blue and red lines represent the high order hinge states. The normalized absolute value of electrical field distribution of the two high order hinge states at $k_z = \pi/p_z$ are illustrated in Figs. 4(a) and 4(b), respectively, where the two types of field patterns with electric field localized in the bottom-right and top-left corner correspond to high order hinge states indicated by blue and red dispersion in Fig. 4(c), respectively. The high order hinge states are continuously distributed among the bandgap and connected to the light cone. The electric field distribution of the high order hinge states is highly confined at the hinge, as shown in Figs. 4(a) and 4(b), which may have potential application in the field of optical sensors.[35,36]

4. Conclusion and perspectives

In conclusion, we have realized TCIs in a judiciously designed photonic metacrystal, which possesses a clean frequency bandgap providing an ideal platform for the studying of surface states. The realistic metacrystal can be fabricated by the standard PCB technique. The topological gapless surface states with quadratic band degeneracy at $\bar{\Gamma}$ point in the (001) surface BZ are protected by C_4 and time-reversal symmetries. The nontrivial bulk band topology is revealed by the Zak phases along bents loops calculated via first-principles calculation. The photonic TCIs exhibit zigzag and gapless surface states along lines from $\bar{\Gamma}$ point to the (001) surface BZ boundary, which are protected by composite operators between time-reversal and glide reflection operators. Our results provide insights into the understanding of nontrivial gapless surface states in photonic TCIs. The surface states emerge at the boundary of the metacrystal and PEC, which provides a route for topologically manipulating light propagation in photonic devices. Moreover, the high order hinge states with highly localized electric fields have potential application in optical sensor.

Acknowledgements

Project supported by the Young Scientists Fund of the National Natural Science Foundation of China (Grant No. 12104148) and the Fundamental Research Funds for the Central Universities (Grant No. 531118010565).

References

[1] Yablonovitch E 1987 *Phys. Rev. Lett.* **58** 2059
[2] John 1987 *Phys. Rev. Lett.* **58** 2486
[3] Yablonovitch, Gmitter and Leung 1991 *Phys. Rev. Lett.* **67** 2295
[4] Vinogradov A P, Dorofeenko A V, Merzlikin A M and Lisyansky 2010 *Phys.-Usp.* **53** 243
[5] Qi M, Lidorikis E, Rakich P T, Johnson S G, Joannopoulos J D, Ippen E P and Smith H I 2004 *Nature* **429** 538
[6] Noda S, Fujita M and Asano T 2007 *Nat. Photon.* **1** 449
[7] Rinne S A, García-Santamaría F and Braun P V 2008 *Nat. Photon.* **2** 52
[8] López C 2003 *Adv. Mater.* **15** 1679
[9] Butt M A, Khonina S N and Kazanskiy N L 2021 *Opt. Laser Technol.* **142** 107265
[10] Kane C L and Mele E J 2005 *Phys. Rev. Lett.* **95** 146802
[11] Bernevig B A, Hughes T L and Zhang S C 2006 *Science* **314** 1757
[12] Wang Z, Chong Y, Joannopoulos J D and Soljačić M 2009 *Nature* **461** 772
[13] Wu L H and Hu X 2015 *Phys. Rev. Lett.* **114** 223901
[14] Yang Y, Gao Z, Xue H, Zhang L, He M, Yang Z, Singh R, Chong Y, Zhang B and Chen H 2019 *Nature* **565** 622

[15] Ozawa T, Price H M, Amo A, Goldman N, Hafezi M, Lu L, Rechtsman M C, Schuster D, Simon J, Zilberberg O and Carusotto I 2019 *Rev. Mod. Phys.* **91** 015006
[16] Chen X D, He X T and Dong J W 2019 *Laser Photon. Rev.* **13** 1900091
[17] Kim M, Jacob Z and Rho J 2020 *Light Sci. Appl.* **9** 130
[18] Huang J, Zhang T, Xu S, *et al.* 2023 *Chin. Phys. Lett.* **40** 047101
[19] Khanikaev A B, Mousavi S H, Tse W K, Kargarian M, MacDonald A H and Shvets G 2013 *Nat. Mater.* **12** 233
[20] Ma T, Khanikaev A B, Mousavi S H and Shvets G 2015 *Phys. Rev. Lett.* **114** 127401
[21] Slobozhanyuk A, Mousavi S H, Ni X, Smirnova D, Kivshar Y S and Khanikaev A B 2016 *Nat. Photon.* **11** 130
[22] Fu L 2011 *Phys. Rev. Lett.* **106** 106802
[23] Yannopapas V 2011 *Phys. Rev. B* **84** 195126
[24] Hsieh T H, Lin H, Liu J, Duan W, Bansil A and Fu L 2012 *Nat. Commun.* **3** 982
[25] Alexandradinata A and Bernevig B A 2016 *Phys. Rev. B* **93** 205104
[26] Alexandradinata A, Höller J, Wang C, Cheng H B and Lu L 2020 *Phys. Rev. B* **102** 115117
[27] Kobayashi S and Furusaki A 2021 *Phys. Rev. B* **104** 195114
[28] Kim M, Wang Z, Yang Y, Teo H T, Rho J and Zhang B 2022 *Nat Commun.* **13** 3499
[29] Liu C X, Zhang R X and VanLeeuwen B K 2014 *Phys. Rev. B* **90** 085304
[30] Lu L, Fang C, Fu L, Johnson S G, Joannopoulos J D and Soljačić M 2016 *Nat. Phys.* **12** 337
[31] Wang H X, Chen Y, Hang Z H, Kee H Y and Jiang J H 2017 *npj Quantum Mater.* **2** 54
[32] Aroyo M I, Kirov A, Capillas C, Perez-Mato J M and Wondratschek H 2006 *Acta Crystallogr. A* **62** 115
[33] Xia L, Guo Q, Yang B, Han J, Liu C X, Zhang W and Zhang S 2019 *Phys. Rev. Lett.* **122** 103903
[34] Long S, Yang J, Wang H Y, Yu Z D, Yang B, Guo Q H, Xiang Y J, Xia L B and Zhang S 2023 *Opt. Lett.* **48** 2349
[35] Schindler F, Cook A M, Vergniory M G, Wang Z, Parkin S S P, Bernevig B A and Neupert T 2018 *Sci. Adv.* **4** eaat0346
[36] Benalcazar W A, Bernevig B A and Hughes T L 2017 *Science* **357** 61